Annals of Physics 355 (2015) 182–203

Contents lists available at ScienceDirect

Annals of Physics

journal homepage: www.elsevier.com/locate/aop

On the inclusion of collisional correlations in quantum dynamics

N. Slama [a], P.-G. Reinhard [b], E. Suraud [a,c,*]

[a] Laboratoire de Physique Théorique, Université Paul Sabatier, CNRS, F-31062 Toulouse Cédex, France
[b] Institut für Theoretische Physik, Universität Erlangen, D-91058 Erlangen, Germany
[c] Physics Department, University at Buffalo, The State University New York, Buffalo, NY 14260, USA

ARTICLE INFO

Article history:
Received 3 November 2014
Accepted 8 February 2015
Available online 17 February 2015

Keywords:
Collisional correlations
Time dependent mean field
Occupation numbers
Single particle entropy
Density matrices

ABSTRACT

We present a formalism to describe collisional correlations responsible for thermalization effects in finite quantum systems. The approach consists in a stochastic extension of time dependent mean field theory. Correlations are treated in time dependent perturbation theory and loss of coherence is assumed at some time intervals allowing a stochastic reduction of the correlated dynamics in terms of a stochastic ensemble of time dependent mean-fields. This theory was formulated long ago in terms of density matrices but never applied in practical cases because of its complexity. We propose here a reformulation of the theory in terms of wave functions and use a simplified 1D model of cluster and molecules allowing to test the theory in a schematic but realistic manner. We illustrate the performance in terms of several observables, in particular global moments of the density matrix and single particle entropy built on occupation numbers. The occupation numbers remain fixed in time dependent mean-field propagation and change when evaluating the correlations, then taking fractional values. They converge asymptotically towards Fermi distributions which is a clear indication of thermalization.

* Corresponding author at: Laboratoire de Physique Théorique, Université Paul Sabatier, CNRS, F-31062 Toulouse Cédex, France.
E-mail address: suraud@irsamc.ups-tlse.fr (E. Suraud).

http://dx.doi.org/10.1016/j.aop.2015.02.008
0003-4916/

1. Introduction

The dynamical description of thermalization in finite quantum systems, following their excitation, is a long standing question. It concerns various fields of physics. It occurs in excitations of clusters and molecules by intense laser fields [1–4] but also for ballistic electron transport in nano systems [5], as well as thermalization in trapped Fermi gases [6], to cite a few prominent examples. Recent advances in the analysis of electronic emission (energy-, angular-resolved distributions, etc.), through elaborate imaging techniques such as Velocity Map Imaging (VMI) [7,8], reveal for the first time crucial details on the dynamics of irradiation in such finite quantum systems [4] and will thus be of key importance for understanding, and ultimately controlling by light, nano systems. Understanding dissipation and thermalization is thus crucial to describe these experiments properly.

Thermalization effects have been explored since long in nuclear physics, especially in induced nuclear fission or nuclear collisions [9,10]. The nuclear case actually provides one of the earliest examples of such investigations, back to the seminal work of Bohr and Wheeler [11]. They pointed out that atomic nuclei can be "heated up" following neutron impact [11]. The generic scenario of such dynamical processes is there very neatly described: the initial energy deposit first provided by neutron hit is progressively redistributed among internal degrees of freedom leading to thermalization of the nucleons. The resulting "hot" nucleus then de-excites via thermal neutron emission and by radiative decay [11]. The example allows to identify the standard phases of the path to thermalization on the basis of "elementary collisional events" which we will from then on call "collisional correlations". The notion of "thermalization" should be taken with a grain of salt. Thermodynamical concepts are developed for infinite bulk. Their application to finite systems requires, in principle, additional consideration [12]. We take here the naive approach and employ standard thermodynamical terms. This is often found sufficient in finite systems if they are not too small, see the above mentioned applications in nuclear physics. The subtleties of finite-size thermodynamics are usually invisible amongst the large fluctuations of the results.

Nuclear theory devoted major efforts since 4 decades to describe thermalization in nuclear reactions, predominantly using semi-classical methods [13,14,10], in line with similar problems in quantum liquids [15,16]. There were attempts to develop improved molecular dynamics methods combining quantum features with a semi classical treatment of dynamical correlations [17,18]. Still, no clear-cut quantum approach is readily available yet, in spite of numerous formal attempts [19,20,10]. The field of clusters and nano structures is far younger but fast developing in relation to the ongoing developments of lasers and imaging techniques. Semiclassical approaches were also considered in the field to include some dynamical corrections [21,22] and could qualitatively describe dynamical processes. But such approaches are bound to simple metals with sufficiently delocalized wave functions, and thus smooth potentials justifying semiclassical approximations. The case of organic systems, in particular the much celebrated C_{60} [4,23], cannot be treated this way. Semi classical, and even classical approaches, can be used at very high excitations such as delivered by very intense laser pulses [2]. In such cases the system is blown up and details of its quantum mechanical features do not matter anymore. But for less violent scenarios, quantum shell effects cannot be ignored.

Although the classical approach is not directly transferable to the quantum mechanical world it is instructive to recall some of its basic aspects. The prototype model equation of non equilibrium dynamics is the Boltzmann equation which provides a microscope picture of the path to thermalization through elementary (local) collisional processes. It has been successfully applied to a wide variety of classical systems [24]. In quantum systems one needs to account for two additional key aspects. On the one hand the uncertainty principle inhibits the notion of local collisions, typical of Boltzmann picture. Furthermore Pauli principle hinders collisions in occupied states. Accounting for both aspects leads to highly involved quantum kinetic equations hardly applicable in realistic finite systems [15,25]. The Pauli principle can be included in the Boltzmann equation in the form proposed by Uehling and Uhlenbeck to deliver the Boltzmann–Uehling–Uhlenbeck (BUU) equation [26], also known as Vlasov–Uehling–Uhlenbeck (VUU) equation. This can be applied to Fermion systems where quantum shell effects are small such as homogeneous Fermion liquids (gases), electrons in solids [5], or nucleons in neutron stars [27]. Furthermore one can consider BUU as the semi classical limit of a quantum kinetic equation, thus applicable to finite Fermion systems under suitable conditions,

typically at large excitations for which quantum shell effects are negligible. This is the way it was used in many applications in nuclear collisions [13,28], in laser excitation of metal clusters [21,22,3], or in electron transport in wires [29].

The high energy range where BUU can be safely used also calls for more than a mere Boltzmann treatment. Indeed, following the basic idea of the fluctuation–dissipation theorem, the higher the excitation/dissipation the larger the fluctuations. This implies in particular that describing the dynamics by a mere kinetic equation is probably insufficient in such highly energetic cases. One then has to proceed to more elaborate approaches in the spirit of Langevin picture. This leads to complement the Boltzmann equation by a Langevin term [30,31], delivering a stochastic kinetic equation. The same line of reasoning in the quantum case leads to stochastic quantum kinetic equations which are formally satisfying but practically impossible to solve in realistic cases. Stochastic extensions were explored in the nuclear case on the basis of the semi classical BUU, again augmenting BUU by a Langevin term [32,33,10,34]. This was in particular used for describing fragmentation scenarios in nuclear collisions [28], which by nature require a multi-exit-channel description. But such approaches, not mentioning their practical involvement, suffer from the same limitations as the BUU equation what concerns the range of applicability and are thus confined to large energies. In electronic systems such investigations beyond the BUU level were not addressed yet. The situation is nevertheless somewhat different in that case, due to the different nature of the system. Indeed, in clusters and molecules the confining potential delivered by the ionic background stabilizes the system for some time and ionization then becomes a highly efficient way to dissipate energy, so that the actual stored excitation energy is regulated by electronic emission. One is then facing a situation where the system is strongly perturbed (thus far away from any equilibrium solution) but with a moderate amount of deposited excitation energy, a typical case where semi classics badly fails. A few "quantum" attempts exist in electronic systems, for example treating correlations at semi classical level on top of quantum mean field [35] in the spirit of Time Dependent Density Matrix approaches [36]. There also exist some rare fully quantum mechanical treatments in schematic model systems [37] and, more practically, in the time-dependent configuration-interaction (TD-CI) method [38]. But these very elaborate treatments remain limited to very small systems and/or low excitations. In spite of its importance a practical quantum dynamical theory of "thermal" effects in molecules and nano clusters thus does not yet exist, to the best of our knowledge. There is thus a clear need for the development of a robust quantum theory of dissipation in finite quantum systems to address the regime of moderate to high excitation energies.

It is the aim of this paper to propose a practical route to attain such a theory on the basis of a purely quantum approach proposed some years ago but never applied in practice. As proof of principle, we shall consider a simple molecular test case. But the approach we propose is generic and can be applied to any finite quantum system exhibiting thermal effects after sizable excitation. The paper is organized as follows. We first recall the original picture and its reformulation in Section 2. The section also serves to introduce basic observables attainable by the theory, in particular beyond mean field. We then propose examples of applications in Section 4, using a simple 1D model tuned to reproduce a typical molecular situation and presented in Section 3. It should be stressed again that, although we consider applications in a molecular case, the proposed theory is by no means limited to such systems. The model parameters are actually flexible enough to cover any other realistic cases such as nuclei or Fermion traps.

2. Formalism

The starting point is Stochastic Time Dependent Hartree–Fock (STDHF) [20] which delivers a description of collisional correlations in terms of an ensemble of TDHF states. The acronym TDHF refers here to the nuclear context in which STDHF was proposed. But the key aspect is rather the fact that the theory is built on time dependent mean field evolution by building up of correlations on top of mean field. This means, in particular, that such a theory is well adapted to physical systems where mean field provides a valuable description of ground state and low energy dynamics. This is typically the case in nuclei (where effective mean-field theory sails under the label "Hartree–Fock"). But this is also true in electronic systems where Density Functional Theory (DFT) [39] provides a robust tool to describe ground state properties and its extension to Time Dependent DFT (TDDFT) is well suited to

simulate the dynamics of electronic systems [40,41]. In terms of mean field the corresponding level of theory is Local Density Approximation (LDA) and its Time Dependent extension TDLDA. The STDHF approach could thus as well be quoted STDLDA in an electronic context. For sake of simplicity, we shall use the acronym STDHF all over the text.

2.1. Density matrix formulation in general

The original formulation of STDHF was done in terms of density matrices which allow simple formal manipulations and to establish connections with standard kinetic theory. Details can be found in [20,10]. We recall here just some key aspects and formula. The idea is to describe correlations in terms of an ensemble of mean field states whose relative weights are evaluated in second order time dependent perturbation theory. In practice we start with an ensemble of $\mathcal{N}$ Slater states $\{|\Phi^{(\alpha)}\rangle, \alpha = 1, \ldots, \mathcal{N}\}$. The associated N-body density matrices of these pure states are denoted $D^{(\alpha)} = |\Phi^{(\alpha)}\rangle\langle\Phi^{(\alpha)}|$. Starting from a given $D^{(\alpha)}$ we then evaluate two-body correlations on top of the TDHF evolution. This is done over a finite time span $\tau_{\rm STDHF}$ long enough to gather a sufficient amount of correlations and short enough to leave mean field the leading component (see also Section 2.2.3). In the general formulation, we assume some expansion basis $|\Phi_\kappa^{(\alpha)}\rangle$ covering the given state and a couple of neighboring Slater states to span the correlated state as $|\Psi^{(\alpha)}\rangle = \sum_\kappa |\Phi_\kappa^{(\alpha)}\rangle c_\kappa$. This yields the correlated N-body density

$$\mathcal{D}^{(\alpha)}(t) = \sum_{\kappa\kappa'} |\Phi_\kappa^{(\alpha)}(t)\rangle c_\kappa(t) c^*_{\kappa'}(t) \langle\Phi_{\kappa'}^{(\alpha)}(t)|. \tag{1}$$

This fully correlated density matrix is very involved. In the standard manner of non-equilibrium statistical physics [25] we argue that the fast phase oscillations in the off-diagonal terms $\kappa \neq \kappa'$ wipe out their contributions in the average. To this end, we consider a sufficient propagation time $t = \tau_{\rm STDHF}$ and reduce then the expansion (1) to diagonal form. This yields the correlated state as an incoherent sum of density operators

$$\mathcal{D}^{(\alpha)}(\tau_{\rm STDHF}) \approx \sum_\kappa w_\kappa^{(\alpha)}(t) D_\kappa^{(\alpha)}(t)\Big|_{t=\tau_{\rm STDHF}}, \qquad D_\kappa^{(\alpha)}(t) = |\Phi_\kappa^{(\alpha)}(t)\rangle\langle\Phi_\kappa^{(\alpha)}(t)|, \tag{2}$$

where $w_\kappa^{(\alpha)} = \left|c_\kappa(\tau_{\rm STDHF})\right|^2$. Evaluating the $c_\kappa(\tau_{\rm STDHF})$ in time-dependent perturbation theory yields an explicit expression for the weight in terms of Fermi's Golden rule [20]

$$w_\kappa^{(\alpha)} = \frac{2\pi\,\tau_{\rm STDHF}}{\hbar} |\langle\Phi_\kappa^{(\alpha)}(t)|\hat{W}|\Phi^{(\alpha)}(t)\rangle|^2 \delta(E^{(\alpha)}(t) - E^{(\kappa)}(t))\Big|_{t=\tau_{\rm STDHF}} \tag{3}$$

for $\kappa \neq \alpha$ and $w_\alpha^{(\alpha)} = 1 - \sum_\kappa w_\kappa^{(\alpha)}$. The term $\hat{W}$ labels the residual interaction beyond mean field, see Eq. (9) and [20]. The energies appearing in the energy matching δ-function above are the ones associated to the mean field states α and κ, respectively. The scheme implies that the mean field provides the dominant component to validate the use of perturbation theory. The choice of the end time $\tau_{\rm STDHF}$ in this expression is somewhat arbitrary. The derivation assumed that the matrix element and the $E(t)$ are only weakly depending on time.

The incoherent correlated state (2) is, in fact, a weighted ensemble of Slater states. When continuing further, each state $D_\kappa^{(\alpha)}$ in this ensemble spawns a further ensemble after the next time step $\tau_{\rm STDHF}$. This will lead quickly to an insurmountable proliferation of states with successively decreasing weights. To keep the scheme manageable, we treat the propagation in terms of an unweighted ensemble with constant number of samples. This is achieved by picking stochastically one Slater state from the ensemble Eq. (2). Thus we generate the new starting point $D^{(\alpha)}$ at $t = \tau^+_{\rm STDHF}$ as

$$\mathcal{D}^{(\alpha)}(\tau_{\rm STDHF}) \longrightarrow D^{(\alpha)}(\tau^+_{\rm STDHF}) = D_\kappa^{(\alpha)} \quad \text{with probability } w_\kappa^{(\alpha)} \tag{4}$$

where $\tau^+_{\rm STDHF}$ symbolizes the new step now starting and the sampling off $w_\kappa^{(\alpha)}$ is done in standard manner using a random number generator.

Under these conditions the further evolution of state α can be continued in terms of another Slater state sampled among the κ according to the weights $w_\kappa^{(\alpha)}$. The final description is attained in terms of the ensemble of thus constructed Slater trajectories which delivers a total (correlated) density matrix

$$\mathcal{D}(t) = \sum_\alpha D^{(\alpha)}(t)/\mathcal{N}. \tag{5}$$

From this correlated density matrix one can directly evaluate average values of observables, as will be discussed below.

It is interesting to note here that by construction STDHF provides an ensemble description of dynamics thus naturally accounting for the effect of fluctuations. From a formal point of view one can show that a proper reformulation of STDHF allows to reduce it to a stochastic kinetic equation of Boltzmann–Langevin type, as discussed above [20]. It thus certainly constitutes a proper starting point for describing dissipative effects in finite quantum systems. We now will reformulate it in a simplified manner in terms of an expansion basis of single-particle (s.p.) states to allow first applications.

2.2. Wave function reformulation and reduction to 2ph excitations

The general, and original, formulation of STDHF leaves a crucial question open, namely the choice of the expansion basis $\{|\Phi_\kappa^{(\alpha)}\rangle\}$. It should be large enough to cover all possibly occurring excitation paths for a given process. It is then obvious that the choice of the basis depends sensitively on the process under consideration. For example, nuclear reactions are extremely demanding in that respect because the wave functions of several fragments have to be taken into account [10]. Dynamics of molecules in strong laser fields leaves usually the system rather compact, at least in the early stages. This is a more forgiving scenario because it allows an STDHF description with rather overseeable basis sets. The compactness limits the fluctuations of the mean field and allows to expand into Slater states built from the s.p. states (occupied and unoccupied) of the actual mean field Hamiltonian. This is the line of realization which we will pursue in the sequel.

2.2.1. The wave function picture

The starting states $|\Phi^{(\alpha)}\rangle$ of the STDHF ensemble are then built from single-particle (s.p.) states $\{\varphi_i^{(\alpha)},\ i = 1\ldots\Omega\}$, where $i = 1,\ldots,N$ stands for the occupied (hole, (h)) states. In addition we complement the hole states by a certain number (sufficient to cover the typical excitation considered) of unoccupied (particle, (p)) states $i = n+1,\ldots,\Omega$. These p states will supply space for the stochastic jumps to come. The enlarged s.p. space provides a simple frame to unfold the hierarchy of n-particle-n-hole (nph) excitations. The first contribution beyond mean field comes with $2ph$ states as $1ph$ excitations are already accounted for in the mean-field ground state and propagation. This is seen by the Thouless theorem saying that every state of the form $|\Phi'\rangle = \exp(\sum_{ph} c_{ph}\hat{a}_p^\dagger\hat{a}_h)|\Phi\rangle$ is again a Slater states if $|\Phi\rangle$ was one [42,43]. True correlations show up with $2ph$ states. We thus take these excited states as

$$|\Phi^{(\alpha)}_{pp'hh'}\rangle = \hat{a}_p^\dagger\hat{a}_{p'}^\dagger\hat{a}_{h'}\hat{a}_h|\Phi^{(\alpha)}\rangle \tag{6}$$

which as such are, again, Slater states, and which we use as the basis for expressing correlations. Starting from an uncorrelated state $|\Phi^{(\alpha)}(0)\rangle$ the propagation will thus deliver a correlated state

$$|\Psi^{(\alpha)}(t)\rangle = |\Phi^{(\alpha)}(t)\rangle + \sum_{pp'hh'} c_{pp'hh'}(t)|\Phi^{(\alpha)}_{pp'hh'}(t)\rangle \tag{7}$$

which at that stage is still coherent. After time τ_{STDHF} we assume loss of coherence and sample $|\Psi^{(\alpha)}(t)\rangle$ in terms of the ensemble of pure Slater states $\{|\Phi_\kappa^{(\alpha)}\rangle, w_\kappa^{(\alpha)}\}$ built as $2ph$ excitations on top of $|\Phi^{(\alpha)}(\tau_{\mathrm{STDHF}})\rangle$. The label κ of the general formulation above is now identified as $\kappa \in \{0, pp'hh'\}$ and the weight $w_\kappa^{(\alpha)}$ becomes $w_\kappa^{(\alpha)} = |c^{(\alpha)}_{pp'hh'}|^2$ which is the probability with which $|\Phi_\kappa^{(\alpha)}\rangle$ appears. Actually, the coherent propagation is evaluated in second order time-dependent perturbation theory

and reduction to an ensemble yields the transition probabilities in terms of Fermi's Golden rule, now for a jump from base state $|\Phi^{(\alpha)}\rangle$ to a $2ph$ excitation thereof $|\Phi^{(\alpha)}_\kappa\rangle$

$$w^{(\alpha)}_{pp'hh'} = \frac{2\pi\,\tau_{\mathrm{STDHF}}}{\hbar}\left|\langle\Phi^{(\alpha)}_\kappa(t)|\hat{W}|\Phi^{(\alpha)}(t)\rangle\right|^2 \delta(\varepsilon^{(\alpha)}_p(t)+\varepsilon^{(\alpha)}_{p'}(t)-\varepsilon^{(\alpha)}_h(t)-\varepsilon^{(\alpha)}_{h'}(t))\Big|_{t=\tau_{\mathrm{STDHF}}} \tag{8}$$

where $\hat{W}$ is again the residual interaction complementing the mean-field Hamiltonian and where the ε are s.p. energies in the mean field of $|\Phi^{(\alpha)}\rangle$. Again, the weight of $|\Phi^{(\alpha)}\rangle$ is the complement $w^{(\alpha)}_\alpha = 1 - \sum w^{(\alpha)}_{pp'hh'}$ and we attribute the weight $w^{(\alpha)}_\alpha$ to the "no transition" case. Similar as in Eq. (3), we evaluate the transition at the end of the step $t = \tau_{\mathrm{STDHF}}$.

It should finally be noted here that the innocent looking term "perturbation theory" becomes in fact rather involved for the present case of TDHF propagation in a self-consistent mean field. We will discuss it in more detail in Section 2.2.3 in connection with an analysis of relevant time scales.

2.2.2. Full ensemble propagation

Now that we have at hand the elementary STDHF step we can construct the ensemble evolution which will provide the tool to actually compute physical observables. The starting point is an initial state $|\Phi_0\rangle$ from which we define each member of the ensemble at initial time as $|\Phi^{(\alpha)}(0)\rangle = |\Phi_0\rangle$. Each member of the ensemble $|\Phi^{(\alpha)}(t)\rangle$ is then propagated individually according to the above discussed scheme, mixing the mean field propagation and the perturbative buildup of correlations. We thus first propagate from 0 to τ_{STDHF} by TDHF/TDLDA. At time τ_{STDHF} one scans all $2ph$ states built on top of $|\Phi^{(\alpha)}(\tau_{\mathrm{STDHF}})\rangle$ to evaluate the jump probabilities $w^{(\alpha)}_\kappa$ following Eq. (8). One then sample the $w^{(\alpha)}_\kappa$'s by randomly choosing one state $|\Phi^{(\alpha)}_\kappa\rangle$ out of the possible κ according to its weight $w^{(\alpha)}_\kappa$. With this new Slater state $|\Phi^{(\alpha)}_\kappa\rangle$ chosen we start again mean field propagation by TDHF/TDLDA from τ_{STDHF} to $2\tau_{\mathrm{STDHF}}$ and again perform another stochastic sampling at time $2\tau_{\mathrm{STDHF}}$ and so on. Once finite time reached the above procedure is restarted from initial time for another member of the ensemble separately. This finally delivers the STDHF ensemble $\{|\Phi^{(\alpha)}(t)\rangle, \alpha = 1,\ldots,\mathcal{N}\}$, whose time evolution can thus be sketched as

$$\left\{\begin{array}{lcccc} |\Phi^{(\alpha)}\rangle & \xrightarrow{TDHF} & \underbrace{\{|\Phi^{(\alpha)}_\kappa\rangle, w^{(\alpha)}_\kappa\}}_{\text{Sampling }\kappa_0} & & \\ & & |\Phi^{(\alpha)}_{\kappa_0}\rangle & \xrightarrow{TDHF} & \underbrace{\{|\Phi^{(\alpha)}_{\kappa'}\rangle, w^{(\alpha)}_{\kappa'}\}}_{\cdots} \\ t=0 & & \tau_{\mathrm{STDHF}} & & 2\tau_{\mathrm{STDHF}} \quad \ldots \end{array}\right\} \alpha = 1,\ldots\mathcal{N}$$

2.2.3. Time scales

In this section, we want to check the conditions which are to be fulfilled for the sampling time τ_{STDHF}, which will also help clarifying the contours of the perturbation theory approximation used in the scheme. To this end, we first need to work out the perturbative computation of correlations in detail. Starting point is the Hamiltonian of the system $\hat{H} = \hat{T} + \hat{V}$ where $\hat{T}$ is the one-body operator of kinetic energy (plus, possibly, an external field) and $\hat{V}$ is a two-body interaction. In (TD)HF theory, it is decomposed into mean-field Hamiltonian $\hat{h}$ and residual interaction $\hat{W}$ as

$$\hat{H} = \hat{h} + \hat{W}, \tag{9a}$$

$$\hat{h} = \sum_{\alpha\beta}\left[T_{\alpha\beta} + \sum_h V_{\alpha h\widetilde{\beta h}}\right]\hat{a}^\dagger_\alpha\hat{a}_\beta, \tag{9b}$$

$$\hat{W} = \frac{1}{2}\sum_{pp'hh'} V_{pp'hh'}\hat{a}^\dagger_p\hat{a}^\dagger_{p'}\hat{a}_{h'}\hat{a}_h + \text{herm.conjg.} \tag{9c}$$

Note that this distinction is defined for a given Slater state $|\Phi\rangle$ and that p, p', h, h' are particle and hole states with respect to this $|\Phi\rangle$. The TDHF propagation is given by (we use here natural units $\hbar = 1$ for the sake of simplicity)

$$\left(\mathrm{i}\partial_t - \hat{h}(t)\right)|\Phi(t)\rangle = 0.$$

It can be resolved formally through the mean-field time evolution operator

$$|\Phi(t)\rangle = \hat{U}(t, t_0)|\Phi(t_0)\rangle, \tag{10a}$$

$$\hat{U}(t, t_0) = \hat{\mathcal{T}}\left\{\exp\left(-\mathrm{i}\int_{t_0}^{t} dt'\hat{h}(t')\right)\right\}, \tag{10b}$$

where $\hat{\mathcal{T}}$ is the time ordering operator [44].

The correlated state $|\Psi\rangle$ obeys the full Schrödinger equation $\mathrm{i}\partial_t|\Psi\rangle = \hat{H}|\Psi\rangle$. We reshuffle it to $\left(\mathrm{i}\partial_t - \hat{h}\right)|\Psi(t)\rangle = \hat{W}|\Psi(t)\rangle$, switch to the interaction picture with $|\Psi(t)\rangle = \hat{U}(t, t_0)|\tilde{\Psi}(t)\rangle$ [44], and integrate over time. This yields the full propagation as integral equation

$$|\tilde{\Psi}(t)\rangle = |\Phi(t_0)\rangle - \mathrm{i}\int_{t_0}^{t} dt'\hat{U}^{-1}(t', t_0)\hat{W}\hat{U}(t', t_0)|\tilde{\Psi}(t')\rangle.$$

Lowest order perturbation theory consists in replacing the $|\tilde{\Psi}(t')\rangle$ on the r.h.s. by the unperturbed initial state $|\Phi(t_0)\rangle$. This yields

$$|\tilde{\Psi}(t)\rangle = |\Phi(t_0)\rangle - \mathrm{i}\int_{t_0}^{t} dt'\hat{U}^{-1}(t', t_0)\hat{W}\hat{U}(t', t_0)|\Phi(t_0)\rangle.$$

The second term on the r.h.s. is identified with the correlation term in Eq. (7). Projecting it onto the explicitly $2ph$ states yields the wanted expansion coefficients explicitly as

$$c_{pp'hh'} = \int_{t_0}^{t} dt'\langle\Phi(t_0)|\hat{a}_h^\dagger\hat{a}_{h'}^\dagger\hat{a}_{p'}\hat{a}_p\hat{U}^{-1}(t', t_0)\hat{W}\hat{U}(t', t_0)|\Phi(t_0)\rangle. \tag{11}$$

This expression cannot be treated further analytically and its numerical computation is also extremely cumbersome. To simplify the expression, we assume, first, that the time evolution of $\hat{h}(t')$ itself is ignorable in the interval $[t_0, t]$, and second, that the mean-field Hamiltonian is approximately diagonal, i.e., $\hat{h} \approx \sum_\alpha \varepsilon_\alpha\hat{a}_\alpha^\dagger\hat{a}_\alpha$. This reduces expression (11) to $c_{pp'hh'} = W_{hh'pp'}\int_{t_0}^{t} dt'\, e^{-\mathrm{i}(\varepsilon_p+\varepsilon_{p'}-\varepsilon_h-\varepsilon_{h'})(t-t')}$. The time integral now separates nicely from the two-body matrix element $W_{hh'pp'}$. We take the absolute squared of this $c_{pp'hh'}$. This allows to evaluate the time integral as

$$\left|\int_{t_0}^{t} dt' e^{-\mathrm{i}(\varepsilon_p+\varepsilon_{p'}-\varepsilon_h-\varepsilon_{h'})(t-t')}\right|^2 = 2\pi(t - t_0)\delta_\Gamma(\varepsilon_p + \varepsilon_{p'} - \varepsilon_h - \varepsilon_{h'}), \quad \Gamma = \frac{1}{t - t_0}. \tag{12}$$

The $\delta_\Gamma(\varepsilon)$ is an approximation to the Dirac δ function with finite energy width Γ which becomes the exact δ function in the limit $\Gamma \longrightarrow 0$. With this time integral together with the spatial matrix element, we obtain finally the jump probability (8) which when divided by the time span $t - t_0$ becomes the jump rate $P^{(\alpha)}_{pp'hh'} = w^{(\alpha)}_{pp'hh'}/(t - t_0)$. Note, however, that the δ function therein is, in fact, a finite-width function δ_Γ.

The above brief derivation has revealed the approximating assumptions on the way to the jump rate. This allows to deduce the following conditions on the sampling time τ_{STDHF} [45] (in natural units $\hbar = 1$):

(1) Perturbative regime: $\tau_{\mathrm{STDHF}} \ll (P_{\mathrm{jump}})^{-1}$
where $P_{\mathrm{jump}} = \sum_{pp'hh'} P_{pp'hh'}$ is the total jump rate and $P_{pp'hh'} = w_{pp'hh'}/\tau_{\mathrm{STDHF}}$.
(2) Slow mean-field: $\tau_{\mathrm{STDHF}} \ll \tau_{\mathrm{mf}}$

where $\tau_{\rm mf}$ is the typical m.f. changing time. This is required to draw $W_{hh'pp'}$ outside the time integral and to ignore the time dependence of ε_α in the dt' integration in Eq. (12).

(3) De-coherence: $(\Delta E_W)^{-1} \ll \tau_{\rm STDHF}$
where ΔE_W = is the energy range covered by $(\hat{W})_{pp'hh'}$. The $(\Delta E_W)^{-1}$ characterizes the de-phasing (de-coherence) time of the exponential kernel in the time integral. Any phase information should have decayed before the next jump.

(4) Dense spectrum: $\tau_{\rm STDHF} \ll 1/\overline{\delta\varepsilon}$
where $\overline{\delta\varepsilon}$ is the average distance between s.p. states. This is required to postpone recurrence of beating in the time integral far beyond the time span between jumps.

Thus we see that the sampling time is bracketed by a couple of typical system times which can be summarized as

$$(\Delta E_W)^{-1} \ll \tau_{\rm STDHF} \ll \tau_{\rm mf},\, 1/\overline{\delta\varepsilon},\, (P_{\rm jump})^{-1}. \tag{13}$$

This shows that we cannot choose arbitrarily any $\tau_{\rm STDHF}$. Leaving out $\tau_{\rm STDHF}$ in the above equation shows that the system times as such impose rigid, but nevertheless plausible, conditions on ΔE_W, the energy range over which the matrix elements $W_{pp'hh'}$ are distributed: $\Delta E_W \gg \tau_{\rm mf}^{-1}$ means it is to be larger than the variance of mean field (=s.p.) energies, $\Delta E_W \gg \overline{\delta\varepsilon}$ means it is to be wider than the mean level distance $\overline{\delta\varepsilon}$, and $\Delta E_W \gg P_{\rm jump}$ means that it is to be larger than the energy uncertainty induced by the finite lifetime of the states. All this has thus to be taken into account when choosing a residual interaction to leave space for a $\tau_{\rm STDHF}$ in between. We shall discuss the impact of the choice of $\tau_{\rm STDHF}$ on a practical example in Section 4.2.

Finally, we remind that the energy resolution of the scheme is given by the finite width $\Gamma = \tau_{\rm STDHF}^{-1}$ and that this is limited from below because $\tau_{\rm STDHF}$ is limited from above. However, taking this serious could easily produce poor energy conservation. In practice, we use Γ as a free numerical parameter to achieve a good compromise between energy conservation and sampling quality. The hope is that reality is often more forgiving than strictly derived bounds.

2.2.4. Practical implementation of the jump probability

The jump rates $w_\kappa^{(\alpha)}$ are central ingredients of the jump probabilities. The realization of the yet formal expression Eq. (8) deserves some words of explanation. We have already seen in the previous section that the Dirac δ-function acquires a finite width Γ, which is a welcome feature for finite systems. These have discrete s.p. spectra which can reasonably be treated only with finite-width selectors. Perturbation theory yields in detail $\delta(\epsilon) \propto \sin^2(\epsilon/\Gamma)/(\epsilon^2\Gamma)$ from the time integral Eq. (12) [46]. This is cumbersome to handle. For better practicability, we approximate that by the box profile Eq. (15b). Moreover, as said above, we are not trying to adjust the width to sampling time $\tau_{\rm STDHF}$. In this first (proof of principle) test case, we employ the width Γ simply as a numerical parameter. One has thus to find a good compromise: Γ has to be larger than the average distance of 2*ph* levels to provide an appropriate coverage of reaction rates and within that restriction it should be as small as possible to ensure sufficient energy stability. We will discuss this point practically on an example in Section 4.2, particularly in Fig. 4.

The s.p. energies entering crucially the δ function in the jump rate Eq. (8) also require some words of caution. They are defined as expectation values $\varepsilon_\alpha = \langle\varphi_\alpha(t)|\hat{h}(t)|\varphi_\alpha(t)\rangle$ and they acquire inevitably some uncertainty $\Delta\varepsilon_\alpha$ in dynamical situations. Even worse, the s.p. energies are ambiguous because a Slater state $|\Phi^{(\alpha)}\rangle$ is by definition invariant under an arbitrary unitary transformation amongst its occupied s.p. states $|\varphi_h^{(\alpha)}\rangle$, $h = 1 \ldots N$. A simple way to minimize these uncertainties is to diagonalize the actual mean field amongst occupied states on the one hand and amongst the unoccupied states on the other hand, which is perfectly legitimate because of the freedom to use these unitary transformations. This means we diagonalize to achieve

$$h_{hh'} = \delta_{hh'}\varepsilon_h, \quad h \le N, \qquad h_{pp'} = \delta_{pp'}\varepsilon_p, \quad p > N. \tag{14}$$

We then use the emerging s.p. states and eigenvalues (with minimal variance) in the jump rate.

Thus far, we have estimated 2*ph* energies exclusively from s.p. energies. For small systems, rearrangement effects on the mean field become important and we need to augment the estimate by a rearrangement-energy $E^{(\mathrm{rearr})}_{pp'hh'}$. This means that we finally use the jump rate in the form (with $\hbar = 1$)

$$w^{(\alpha)}_{pp'hh'} = 2\pi\,\tau_{\mathrm{STDHF}} \left|\langle \Phi^{(\alpha)}_{pp',hh'} | \hat{W} | \Phi^{(\alpha)} \rangle\right|^2 \delta_\Gamma(\varepsilon^{(\alpha)}_p + \varepsilon^{(\alpha)}_{p'} - \varepsilon^{(\alpha)}_h - \varepsilon^{(\alpha)}_{h'} + E^{(\mathrm{rearr})}_{pp'hh'}), \tag{15a}$$

$$\delta_\Gamma(\epsilon) = \vartheta(\epsilon - \Gamma)\vartheta(\Gamma - \epsilon)/2\Gamma, \tag{15b}$$

where ϑ is the Heaviside function. The rearrangement energy $E^{(\mathrm{rearr})}_{pp'hh'}$ becomes negligible in large systems because changing two states out of hundredth of particles will not matter much. However, it cannot be ignored in small systems such as our test case. Practically speaking, this means that, rather than filtering possible transitions only in terms of single particle energies, we further explicitly check that a transition is possible in terms of total energy, which amounts to include the rearrangement energy in the above δ function.

2.3. Density matrices, observables and variances

The STDHF formalism immediately gives access to correlated density matrices, by summing up the ones associated to Slater states (which take simple forms), following the general rule given by Eq. (5). In this section, we consider observables which can be computed from one- and two-body density matrices. We will do that in real space representation and use the abbreviations $\mathbf{r}_1 \equiv 1$, $\mathbf{r}_{1'} \equiv 1'$, and similarly for other labels. This will deliver a better readable, compact form of the space integrals.

2.3.1. One- and two-body density matrices

The information on one-body observables is contained in the one-body density matrix, sampled as

$$\rho(1;1') = \langle \hat{\psi}^\dagger(1')\hat{\psi}(1)\rangle = \frac{1}{\mathcal{N}}\sum_\alpha \rho^{(\alpha)}(1;1'), \tag{16a}$$

$$\rho^{(\alpha)}(1,1') = \sum_{h=1}^{N} \varphi^{(\alpha)}_h(1)\varphi^{*(\alpha)}_h(1') \tag{16b}$$

where $\hat{\psi}$, $\hat{\psi}^\dagger$ are Fermion operators and the last summation runs over hole states h only. All information on two-body correlations is contained in the two-body density operator

$$\rho_2(1,2;1',2') = \langle \hat{\psi}^\dagger(1')\hat{\psi}^\dagger(2')\hat{\psi}(1)\hat{\psi}(2)\rangle = \frac{1}{\mathcal{N}}\sum_\alpha \rho^{(\alpha)}(1,2;1',2'), \tag{17a}$$

$$\rho^{(\alpha)}_2(1,2;1',2') = \rho^{(\alpha)}(1,1')\rho^{(\alpha)}(2,2') - \rho^{(\alpha)}(2,1')\rho^{(\alpha)}(1,2') \tag{17b}$$

which takes a trivial form for Slater states (17b). The full two-body matrix is rather bulky. In the following we consider only local one-body operators and products thereof. Thus we will rather use the density–density correlation function [44]

$$\Pi(1,2) = \langle \hat{\psi}^\dagger(1)\hat{\psi}(1)\hat{\psi}^\dagger(2)\hat{\psi}(2)\rangle = \rho_2(1,2;1,2) + \delta(1,2)\rho(1,2). \tag{18}$$

2.3.2. Expectation values and variances of one-body operators

A general one-body operator in coordinate-space representation is given as a matrix $A(1,1')$. Its expectation value then becomes $\overline{A} = \int d1d1' A(1,1')\rho(1',1)$. We consider here the simpler case of local operators $A(1,1') \longrightarrow A(1)\delta(1,1')$. The expectation value reads

$$\overline{A} = \int d1 A(1)\rho(1,1). \tag{19}$$

The expectation value of the squared (local) operator becomes

$$\begin{aligned}\overline{A^2} &= \int d1\, d2\, A(1)A(2)\Pi(1,2) \\ &= \int d1\, d2\, A(1)A(2)\rho_2(1,2;1,2) + \int d1\, A(1)^2\rho(1;1). \end{aligned} \tag{20}$$

From that one can compute the variance as

$$\begin{aligned}\overline{\Delta^2 A}^{(\mathrm{full})} &= \overline{A^2} - (\overline{A})^2 \\ &= \int d1\, d2\, A(1)A(2)\rho_2(1,2;1,2) + \int d1\, A(1)^2\rho(1;1) \\ &\quad - \left(\int d1\, A(1)\rho(1;1)\right)^2. \end{aligned} \tag{21}$$

It is instructive to consider this variance for one sample, i.e. for a pure Slater state. In that case, we have

$$\rho_2^{(\alpha)}(1,2;1',2') \longrightarrow \rho^{(\alpha)}(1,1')\rho^{(\alpha)}(2,2') - \rho^{(\alpha)}(2,1')\rho^{(\alpha)}(1,2').$$

The variance for this pure independent-particle (mean field) state then reduces to

$$\overline{\Delta^2 A}^{(\alpha)} = \int d1\, A^2(1)\rho^{(\alpha)}(1;1) - \int d1 d2\, A(1)A(2)\rho^{(\alpha)}(1,2)\rho^{(\alpha)}(2,1). \tag{22}$$

This shows that already a pure independent-particle state has a certain variance. The full variance (21) thus consists in a (coherent) quantum mechanical background and a contribution from the incoherent, statistical correlations. The ensemble averaged quantum-mechanical correlations are

$$\begin{aligned}\overline{\Delta^2 A}^{(QM)} &= \frac{1}{\mathcal{N}}\sum_\alpha \overline{\Delta^2 A}^{(\alpha)} \\ &= \int d1\, A^2(1)\rho(1;1) - \int d1 d2\, A(1)A(2)\frac{\sum_\alpha \rho^{(\alpha)}(1,2)\rho^{(\alpha)}(2,1)}{\mathcal{N}}. \end{aligned} \tag{23}$$

We decompose then the full squared variance as

$$\overline{\Delta^2 A}^{(\mathrm{full})} = \overline{\Delta^2 A}^{(QM)} + \overline{\Delta^2 A}^{(\mathrm{incoh})} \tag{24}$$

where the remaining $\overline{\Delta^2 A}^{(\mathrm{incoh})}$ part carries the contribution from incoherent statistical averaging, which can be rewritten as

$$\overline{\Delta^2 A}^{(\mathrm{incoh})} = \frac{1}{\mathcal{N}}\sum_\alpha \overline{A}^{(\alpha)}\overline{A}^{(\alpha)} - \left(\frac{1}{\mathcal{N}}\sum_\alpha \overline{A}^{(\alpha)}\right)^2. \tag{25}$$

The incoherent part summarizes the variance of expectation values in the ensemble. We shall see illustrative examples in Sections 4.3 and 4.4. What we call henceforth variance is then the square root of these expressions, e.g., $\overline{\Delta A}^{(\mathrm{full})} = \sqrt{\overline{\Delta^2 A}^{(\mathrm{full})}}$.

2.3.3. Analysis of thermal effects

As one of the goals of STDHF is to account for dissipative effects and thermal features it is interesting to introduce measures of thermalization. For this purpose we start again from the one-body density matrix of the STDHF ensemble that we rewrite as

$$\hat{\rho} = \frac{1}{\mathcal{N}}\sum_{\alpha=1}^{\mathcal{N}}\sum_{i=1}^{N} |\varphi_i^{(\alpha)}\rangle\langle\varphi_i^{(\alpha)}| \equiv \sum_\nu |\varphi_\nu^{(\mathrm{nat})}\rangle n_\nu \langle\varphi_i^{(\mathrm{nat})}|. \tag{26}$$

We have introduced here a representation of the one-body density matrix in terms of the natural s.p. orbitals $|\varphi_\nu^{(\mathrm{nat})}\rangle$ which diagonalize $\hat{\rho}$. The eigenvalues are then the occupation numbers n_ν of the natural orbitals and their distribution can be plotted as a function of s.p. energy. The summation runs over the ν eigenvalues accessible through our actual representation of the one-body density matrix. In the following applications we use a grid representation so that the summation runs over the number of mesh points used in the computations.

Occupation numbers do provide a natural tool for analyzing thermal effects. Remind that in a pure Slater state they remain exactly equal to 1 (hole state) or 0 (particle state) and do not depend on time. In the case of the STDHF one-body density matrix, occupation numbers n_ν do take fractional values and evolve in time. If starting from a Slater state, as outlined above, one expects to reach an asymptotic Fermi-like profile of these occupation numbers once thermalization has been reached. We shall illustrate the case in Section 4.1.2.

Occupation numbers also provide the natural input to evaluate the one-body entropy

$$S = -k_B \sum_\nu [n_\nu \log n_\nu + (1 - n_\nu) \log(1 - n_\nu)] \tag{27}$$

where k_B is the Boltzmann constant. It characterizes the approach to thermal equilibrium and thus allows to estimate microscopic relaxation times. The one-body entropy S provides a compact measure of the time evolution of thermal properties of the system. We shall use it at many places in the following, in particular to test the possible impact of parameters of the theory, see in particular Section 4.2.

3. A simple 1D model

The aim of this paper is to test the capabilities of STDHF in realistic dynamical situations. To that end, we have chosen to develop a simple 1D model mimicking a molecular/cluster case. Its mean field Hamiltonian is given as (x representation, $\hbar = 1$)

$$\hat{h}^{(\alpha)} = -\frac{\Delta}{2m} + V_{ext}(x) + \lambda \left(\varrho^{(\alpha)}(x)\right)^2, \tag{28a}$$

$$V_{ext}(x) = \frac{V_0}{1 + \exp\left(\frac{x - y_0}{a}\right)} + \frac{m\omega^2}{2}(|x| - y_0 - 2a)^2 \theta(|x| - y_0 - 2a), \tag{28b}$$

$$\varrho^{(\alpha)}(x) = \sum_{i=1}^{N} |\varphi_i^{(\alpha)}(x)|^2, \tag{28c}$$

where $\varrho^{(\alpha)}(x)$ is the local one-body density associated to the actual Slater state $|\Phi^{(\alpha)}\rangle$. The external potential $V_{ext}(x)$ is to represent a typical ionic background of a simple molecule/atom ($V_0 = -5$ Ry, $y_0 = 15$ a$_0$, $a = 2$ a$_0$) complemented by a confining harmonic oscillator with $\omega = 4$ Ry, tailored to act only outside the potential well ($|x| > y_0 + 2a$). This confining potential ensures soft reflecting boundary conditions. Closing the system this way avoids the conceptual complications of non-equilibrium thermodynamics in open systems. The self-consistent term $\propto \lambda$ serves to simulate a typical self-consistent mean-field (HF or LDA) and its impact (relative to $V_{ext}(x)$) can be tuned with λ. The two-body interaction beyond the $\left(\varrho^{(\alpha)}(x)\right)^2$ is zero-range potential $\delta(x - x')$, formally similar as the one used for the residual interaction. In the present molecular case we use a moderate self consistent term with $\lambda = 2$ Ry a$_0^2$. The set of chosen mean-field parameters leads to a sufficiently dense spectrum of s.p. energies which is important to produce a sufficient number of 2ph transitions.

The residual interaction $\hat{W}$ ought to describe the in-medium scattering cross section and has usually to be taken as the screened two-body interaction [47–49]. For the present exploratory test case it has been chosen as a simple contact force $W(x, x') = W_0 \delta(x - x')$ with $W_0 = 1.3$ Ry. This choice leads to realistic relaxation times for the entropy (see below).

In the following we will apply this simple model to $N = 9$ physical particles having the same spin. Our space thus contains 9 hole states and an arbitrary number $\Omega - N$ of particle states. We shall check

the impact of the latter number in Section 4.2. As a first analysis of the dynamics of this system, we have checked its optical response. The dominant optical transition has an associated period in the fs range (actually 1.15 fs), which is typical of clusters and molecules. The STDHF time scale is chosen following [20] as $\tau_{\mathrm{STDHF}} = 1$ fs. We shall see in Section 4.2 that this choice is legitimate. In most calculations we follow the dynamics over 100 fs which is long enough for thermal relaxation studies and much shorter than the Poincaré recurrence time of the model [50]. The typical STDHF ensemble has $\mathcal{N} = 100$ members, which for sufficient excitation energies (and thus transition probabilities) is enough to keep statistical fluctuations at an acceptable low level (see also the discussion in Section 4.2).

The stationary state is obtained by solving the static mean-field equations with the Hamiltonian (28). We then initialize the dynamics by an instantaneous multi-particle–hole excitation. This simple excitation model allows best to concentrate on jumps and thermalization as it avoids interference with coherent excitations (in case of dipole boost) and external time scales (laser irradiation). The *ph* states are chosen randomly. This delivers various initial excitations at different excitation energies E^*. To span the space of lower energies, we use 1*ph* excitations. For larger energies, we step up to 2*ph* states and even more, if wanted, is obtained by higher *ph* states. This simple and clean way to excite the system leads quickly to a sufficient number of level crossings between occupied and unoccupied levels and with it a sufficient number of 2*ph* transitions which match the δ_Γ function in the rate (8). This, in turn, delivers sufficiently large total transition probabilities (up to some tens of % at most), which suffices to allow good statistics of jumps, while keeping the dynamics in the weak coupling regime.

4. Results

4.1. How it works

4.1.1. Evolution of energies

The STDHF scheme requires dynamical scenarios where 2*ph* "excitations" about a given Slater state do not really require additional excitation energies, but can take place at near zero energy difference with the given energy width Γ (Section 2.2.4). To get an idea how such situations could emerge, we show in Fig. 1 the time evolution of s.p. energies for the case of an initial 1*ph* excitation with excitation energy $E^* = 1.9$ Ry. We compare results from a pure TDHF/TDLDA propagation (upper panel) with those from one member of the STDHF ensemble (lower panel). This allows also to illustrate the differences between TDHF and STDHF. Both cases start from the same configuration. One sees clearly the 1*ph* structure at initial time. In case of pure TDHF, the s.p. energies fluctuate a bit, but maintain basically their ordering. Occupation numbers are frozen at their original $n_\alpha = 1$ or 0 values (thus with an occupied state above empty ones and a deeply lying empty state) and the entropy thus remains zero all time. STDHF, on the other hand, occasionally exploits one of the many level crossings between occupied and unoccupied levels which develop in the course of time. This gives rise to situations in which the 2*ph* energy entering Eq. (8) becomes zero thus allowing a jump into a new configuration. The jumps are indicated by dashed blue vertical lines in the lower panel of Fig. 1. The density of these events is not overwhelmingly large in this rather small test case, but suffices to produce a sufficient amount of jumps. Systems with more particles and in higher dimensions will deliver a much higher density of level crossings thus producing even smoother results than we will see for the present case. Each sample of the STDHF ensemble will have a different sequence of (stochastic) jumps. This produces a mixed state in the ensemble average and steady growth of entropy, see for example Fig. 4.

Energy preservation along the dynamics is a delicate issue. Because we use a finite width Γ in Eq. (8) we will observe some spread of energies due to the finite energy band allowed in the stochastic jumps. This is demonstrated in Fig. 2 where we plot the time evolution of total energies for the ensemble average and variance for STDHF dynamics at an excitation energy of $E^* = 3.1$ Ry. We have chosen this case as most critical as smaller excitation energies lead to smaller effects. This shows clearly how spreading evolves along the time evolution. One can also see a slight trend to increasing average energy. This global drift is due to the fact that the phase space of 2*ph* states is larger at the side of higher energies. Both effects, spreading and trend, remain sufficiently small within the observation

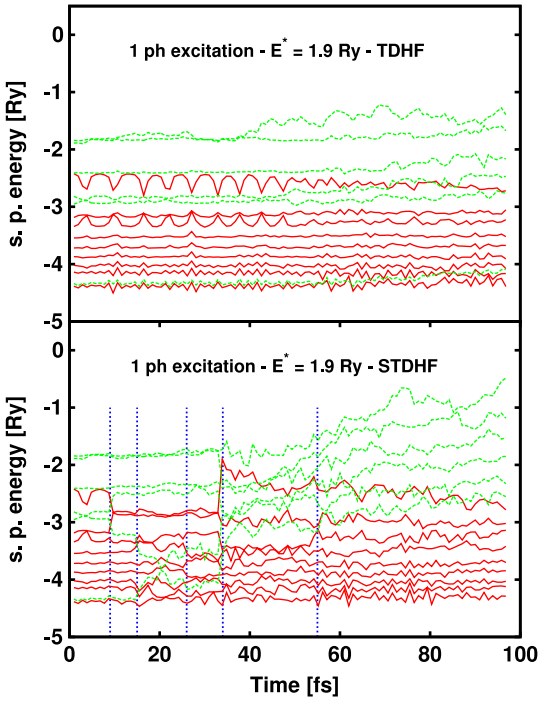

Fig. 1. Time evolution of s.p. energies after an initial 1*ph* excitation with energy $E^* = 1.9$ Ry for case of pure TDHF (upper) and for one member of the STDHF ensemble (lower). Occupied states are drawn with solid (red) lines and unoccupied ones with dashed (green) lines. The vertical dashed blue lines indicate where 2*ph* jumps occurred in the STDHF case. We have used here $\Gamma = 0.1$ Ry. (For interpretation of the references to color in this figure legend, the reader is referred to the web version of this article.)

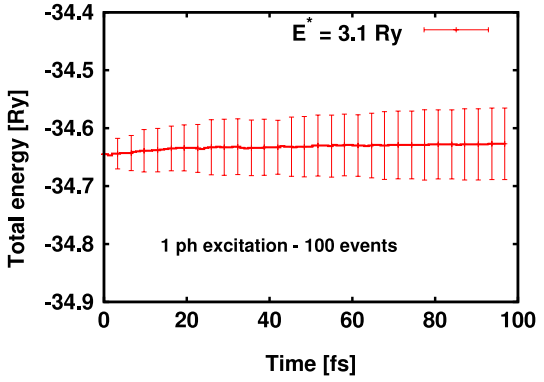

Fig. 2. (Color online) Time evolution of ensemble average and variance of total energies of STDHF events after an initial 1*ph* excitation with excitation energy $E^* = 3.1$ Ry. We have used here $\Gamma = 0.1$ Ry.

time. This validates our present approach which does not yet include specific measures for energy restoration.

4.1.2. Relaxation processes

A major issue for STDHF is to analyze the relaxation dynamics of an excited quantum system through collisional correlations. As outlined in Section 2.3.3, this can be analyzed easily in terms of

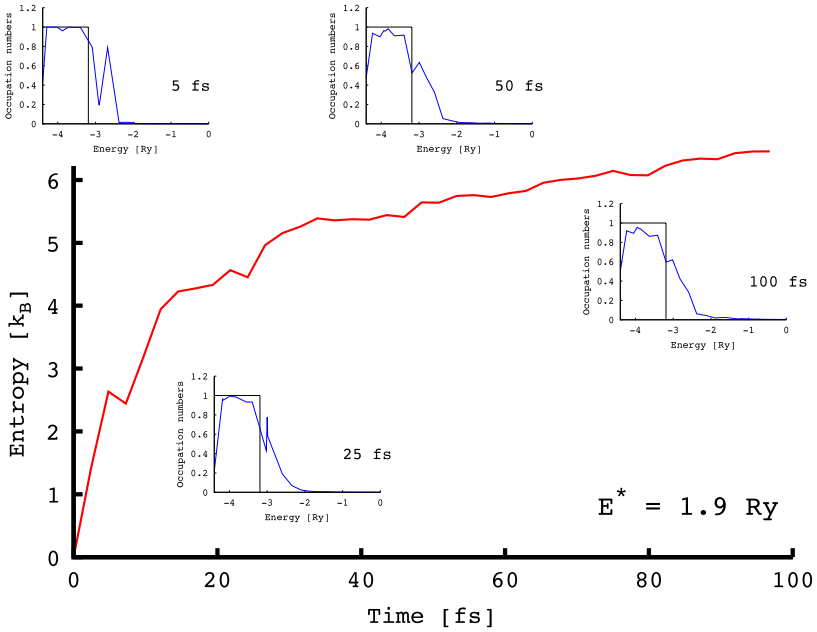

Fig. 3. Time evolution of the one-body entropy after a 1*ph* excitation delivering an excitation energy of 1.9 Ry. Also are plotted as insets the actual distributions of s.p. energy occupation numbers at a few illustrative times, 5, 25, 50 and 100 fs. The initial hole is still clearly visible at time 5 fs and is gradually filled in the course of the dynamics. We have used here $\Gamma = 0.1$ Ry and $\mathcal{N} = 100$ events.

occupation numbers n_ν of the natural orbitals (Eq. (26)). Having obtained these occupation numbers then provides a simple measure of the relaxation process in terms of the one-body entropy S (Eq. (27)). We illustrate the point in Fig. 3 where we plot the time evolution of S in the case of an initial excitation of 1.9 Ry. For completeness we also plot a few snapshots of the energy distribution of the n_ν. The excitation energy is deposited in this case via an instantaneous 1*ph* excitation (Section 3). It is interesting to see how the thus created initial hole is still clearly visible at time 5 fs and is gradually filled in the course of the dynamics, an effect which of course would not occur in a pure TDHF evolution. The entropy accordingly increases in time exhibiting two regimes: at short time one observes a rather quick relaxation followed by a slower one on longer times. This typically corresponds to the expected behavior in a system relaxing towards thermal equilibrium. The proximity to thermalization is also visible from the distribution of occupation numbers at time 100 fs where we see that the shape of the distribution does clearly approach the expected Fermi factor. A systematic analysis of this relaxation dynamics within STDHF was already performed elsewhere and we thus refer the reader to this reference for more details [51].

4.2. Impact of key parameters

In this section, we perform a few technical checks to validate the typical parameters chosen to describe the STDHF dynamics. We successively consider the impact of the finite width Γ of the energy δ function in Eq. (15), the impact of the sampling time τ_{STDHF}, the effect of size of the set of particle states used in the simulations and finally consider the impact of the size of the stochastic ensemble.

As already indicated in Section 2.2.4, in this first (proof of principle) test case, we simply employ the width Γ as a numerical parameter to allow collisions in a discrete spectrum, without affecting energy conservation too much. As already noted Γ should be larger than the average distance of excitation levels. In the present 1D model the level distance typically varies between 10^{-4} and 2.5 10^{-3} Ry, in the range of excitation energies we have explored. On the other hand, a small Γ is preferable for minimal

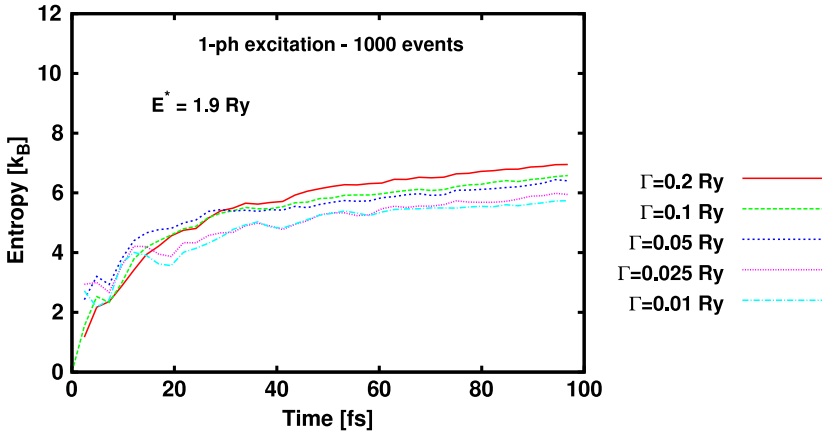

Fig. 4. Evolution of entropy as a function of time for various values of Γ.

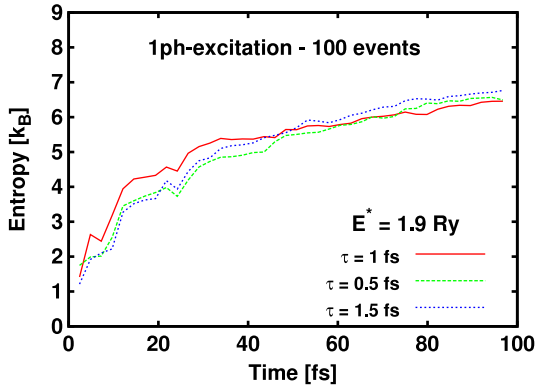

Fig. 5. Evolution of entropy as a function of time for various values of τ_{STDHF}.

violation of energy conservation. Fig. 4 shows the time evolution of entropy for a broad choice of values of Γ. Larger Γ yields slightly larger entropy. However, the dependence is very weak. The same weak dependence is found for the final occupation distributions (not shown here). We have also looked at the number of collisions as a function of Γ and find that it is rather stable up to $\Gamma = 0.1$ Ry turning to moderate growth above that value. Thus we can conclude that the actual choice of Γ is not so critical. All values up to $\Gamma = 0.1$ Ry are acceptable. Very small values of Γ require larger samples. Note that in Fig. 4 we have taken a sampling of 1000 events precisely to ensure proper statistical convergence for very small Γ's. Thus we choose $\Gamma = 0.1$ Ry as the standard value for our present studies. We have seen in Fig. 2 that this choice still provides acceptable energy conservation.

The impact of the sampling time τ_{STDHF} is analyzed in Fig. 5. Our standard value is $\tau_{\text{STDHF}} = 1$ fs, which matches basic STDHF requirements (Section 2.2.3). In order to validate this choice, we have tested two other values also compatible with STDHF requirements namely $\tau_{\text{STDHF}} = 0.5$ fs and $\tau_{\text{STDHF}} = 1.5$ fs. The impact of τ_{STDHF} on the sensitive one-body entropy S is shown in Fig. 5. Up to details, which can be attributed to statistical effects, the results obtained are very similar. This means that the results are robust within a certain range of values of τ_{STDHF}, as expected on formal grounds [20]. This also a posteriori validates the applicability of STDHF in this test case.

The next check is somewhat more technical, related to the number of particle states included in the description of the system. Its choice is dictated by the actual excitation energy delivered to the system, the larger the excitation energy, the higher the energy of possibly attained s.p. levels and

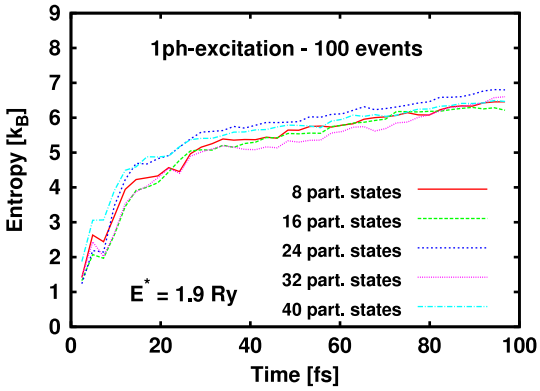

Fig. 6. Evolution of entropy as a function of time for various values of the number of empty states.

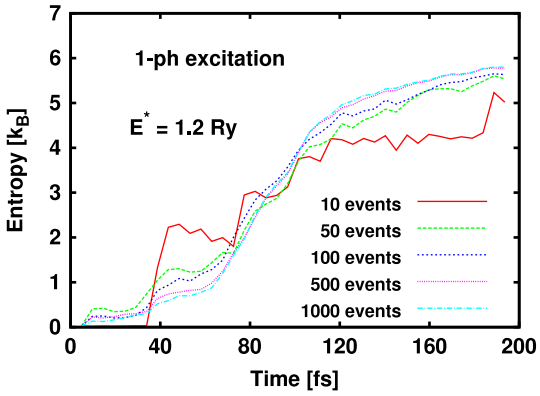

Fig. 7. Time evolution of entropy for $E^* = 1.2$ Ry and various numbers of events.

thus the larger the number of particle states to be included in the description of the system. Of course, increasing the number of empty states rapidly affects computational cost so that it is a parameter to be optimized for obvious practical reasons. We show in Fig. 6 the impact of the number of particle states on the evolution of the one-body entropy S in an example at an excitation energy of 1.9 Ry, typical of the ones used in this work. The impact is clearly marginal. In the following we have thus used the smallest value of the number of particle states, namely eight in this case, to save computational time.

Finally we want to address the impact of statistics. By construction a stochastic approach requires good statistics to attain a proper level of accuracy. At high excitation energies, the large number of $2ph$ transitions naturally provides a large number of transitions and thus allows to achieve good statistics at an affordable computational price. This becomes more critical for lower excitation energies where the decreasing number of $2ph$ transitions requires increasingly larger ensembles to ensure proper sampling. It is thus important to explore that limit. Fig. 7 illustrates the case on the smallest excitation energy we have considered here namely for $E^* = 1.2$ Ry. It shows nicely a convergence towards the asymptotic entropy profile. However, convergence is rather slow for this low excitation, requiring hundredths of events. The next case (not shown here) at $E^* = 1.9$ Ry already provides convergence for 100 events and convergence becomes even better for larger excitation energy.

4.3. One and two-body density matrices

We now want to analyze the behavior of one- and two-body density matrices (defined in Section 2.3.1). In order to analyze their time evolution in simple terms we restrict the analysis of

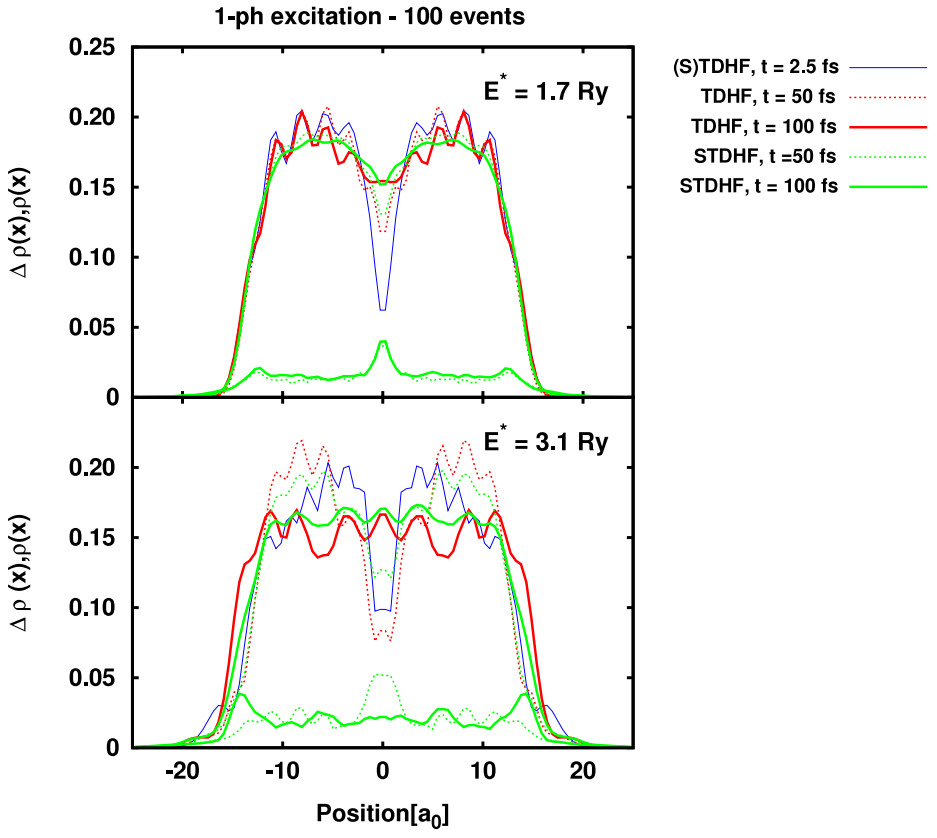

Fig. 8. Density $\varrho(x)$ (upper curves) and associated variance $\Delta\varrho(x)$ (Eq. (29)) as a function of time for TDHF and STDHF evolution and an excitation energy $E^* = 1.7$ Ry (upper panel) and $E^* = 3.1$ Ry (lower panel, lower curves).

one-body density matrices to the local density $\varrho(x)$, which is its diagonal part, and to the associated incoherent variance Eq. (25), which specifically reads in that case:

$$\Delta\varrho(x) = \sqrt{\overline{\Delta^2\varrho(x)}^{(\text{incoh})}} = \sqrt{\frac{1}{\mathcal{N}}\sum_\alpha \rho^\alpha(x)^2 - \left(\frac{1}{\mathcal{N}}\sum_\alpha \rho^\alpha(x)\right)^2}. \tag{29}$$

The time evolution of $\varrho(x)$ and its $\Delta\varrho(x)$ is shown in Fig. 8 for two excitation energies, $E^* = 1.7$ Ry and $E^* = 3.1$ Ry. The upper curves in each panel correspond to the density while the lower ones correspond to the variance. Both TDHF and STDHF are considered. As expected one observes that the STDHF description leads to a much smoother density profile than the TDHF one, due to thermalization. The point is confirmed by the values of the variance $\Delta\varrho(x)$. As expected, the TDHF variance remains zero while the STDHF variance acquires sizable values everywhere.

It is interesting to complement the analysis of the one-body density by considering the two-body density matrix. It is rather bulky, even when simplified to $\rho_2(x, y; x, y)$ and in a 1D setup. For the sake of simplicity and clarity we consider only a cut through it. The interesting case is the second diagonal $\rho_2(x, R - x; x, R - x)$ of the computational box of size R, which directly passes through the correlation hole line $x = y$, where ρ_2 is exactly zero by construction. This cut is shown in Fig. 9. Again we compare TDHF and STDHF time evolution along the second diagonal of the computational box. We observe similar pattern as in the case of the one-body density namely the fact that the STDHF evolution leads to much smoother profiles than the TDHF one, again an expected effect.

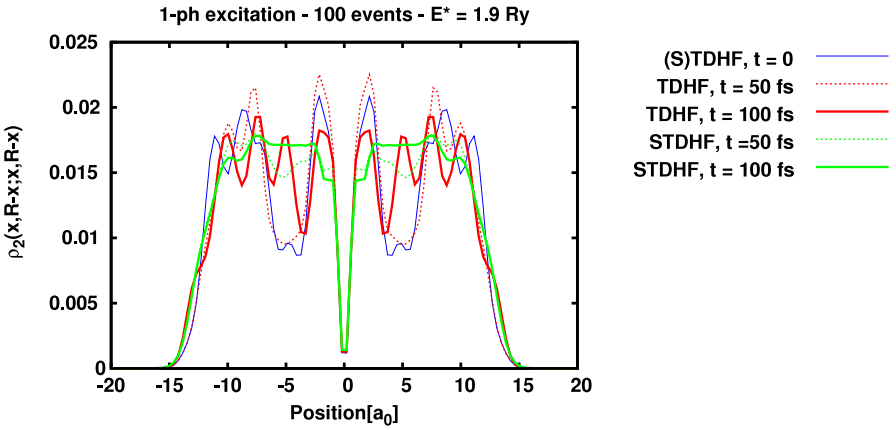

Fig. 9. Cut of the two-body density matrix $\rho(x, y; x, y)$ along the line $y = R - x$ (where R is box radius) for an excitation energy $E^* = 1.9$ Ry.

4.4. Global observables

The analysis of densities is very detailed but does not allow to display the time evolution in a simple fashion. This goal can be better achieved by using integrated observables and their variances, as discussed in Section 2.3.2. In that spirit, we consider here the monopole and dipole moments of the system.

We first consider the case of the square radius or monopole, which amounts to choose as operator

$$A(x) \longrightarrow M = x^2 - x_0^2 \tag{30}$$

where $x_0 = \bar{x}^2(t = 0)$ (Eq. (19)) is the r.m.s. radius of the initial ground state. Results are shown in Fig. 10 for the various quantities introduced in Section 2.3.2, namely the "Full" variance, as computed from Eq. (21), the "QM" variance from Eq. (23) and the "incoherent" variance computed as the difference between "full" and "QM" variances. All quantities are drawn in units of x_0^2, i.e. in units of system size. The value of M as such (panel a) shows only small fluctuations in the course of time. There are no marked regular oscillations. This is due to the particular excitation process by *nph* states which is designed to deliver at once a strong stochastic perturbation without causing large collective motion. The quantum mechanical part of the variance (panel c) is the dominating contribution. It also has a large offset which grows with initial excitation energy. It also grows slightly in time, but the growth is a tiny fraction of the initial offset. The same trend is seen in the full variance (panel b), which is obvious as this is mainly given by the QM part. The incoherent part (panel d) is much smaller. But relative to its small initial values, we see a larger growth in the course of time. This is plausible because the incoherent part is driven by thermalization of the system.

Fig. 11 compares STDHF to TDHF results for M and its variances. The comparison is done for two excitation energies. The values of M as such were already rather stable with only small fluctuations in STDHF. They show even much less fluctuations for pure TDHF which again is typical for the chosen way of *nph* excitation. The QM variances from STDHF are somewhat larger than those from TDHF. This is due to the fact that STDHF distributes the excitation over several states, many of them with larger intrinsic variance. A huge difference is seen, of course, for the incoherent variance. STDHF has some contribution from it, although smaller than the leading part of the QM variance, while by construction TDHF does not possess such a variance. The full variances from TDHF are thus fully determined by the QM variances. The full STDHF variances gather a bit from the incoherent contributions. This example of the monopole moment shows that thermodynamic features are hard to identify from global observables. The detailed observables of occupation numbers (Section 4.1.2) and of density distributions (Section 4.3) are much more sensitive in that respect.

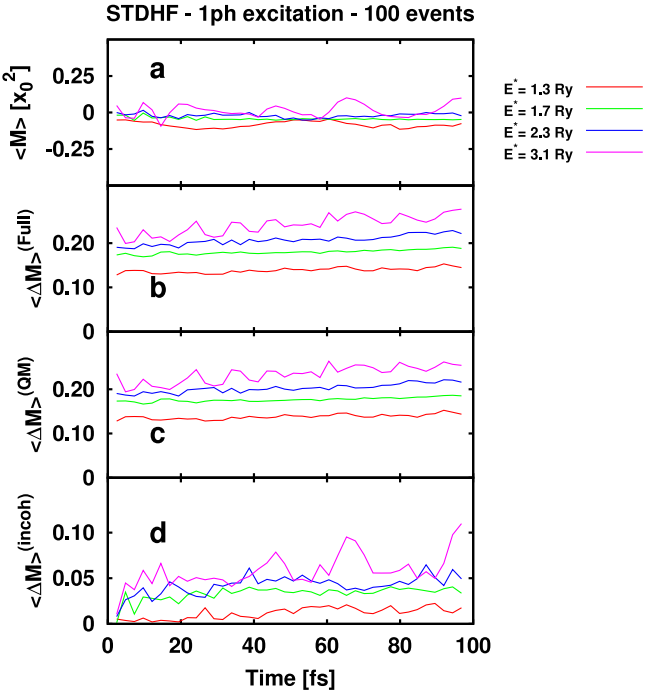

Fig. 10. Time evolution of variances of the "monopole moment" M defined in Eq. (30) for various excitation energies as indicated. Panel a displays M as such for reference. Panel b displays the "Full" variance, as computed from Eq. (21), panel c the "QM" variance from Eq. (23) and panel d the "incoherent" variance computed as the difference between "full" and "QM" variances. All quantities are drawn in units of the mean square radius x_0^2 which is the natural unit for M.

We finally consider the case of the dipole operator

$$A(x) \longrightarrow d = x. \tag{31}$$

This is the center of mass of the electron cloud. Our *nph* excitations starts at $d = 0$ and let also the total momentum of the cloud at zero (= at rest). Thus d should continue to stay zero all time. Fig. 12 shows the time evolution of d and its variances for STDHF propagation at various excitation energies. The average d (panel a) stays indeed zero for a while, but acquires some fluctuations later on. Remind that we are not forcing momentum conservation in the present scheme. Thus fluctuations can arise. But it is gratifying that they stay so low. Particularly satisfying is that there is no global drift in d. The values fluctuate about zero. The remaining fluctuations indicate the incompleteness of our sampling. They could be suppressed more by enhancing the size of the STDHF ensemble. The fluctuations moreover increase with decreasing excitations energy with particularly larger values for the lowest E^*. This demonstrates that sampling becomes the more cumbersome the smaller the excitation.

The variances of dipoles d behave very similar to what we had seen already for the monopoles M. The QM contribution dominates. Here, the incoherent part contributes even less than in case of M. Moreover, the time pattern of the incoherent part of d differ from that of M. They show a delayed start of growth and, once started, a nearly linear growth.

5. Conclusion

In this paper, we have investigated an extension of time-dependent mean-field theory (called Time-Dependent Hartree–Fock = TDHF) by dynamical correlations through electron–electron collisions. The correlations are handled in terms of an ensemble of TDHF states accounting for the correlations by stochastic jumps between configurations. Thus we call this approach stochastic

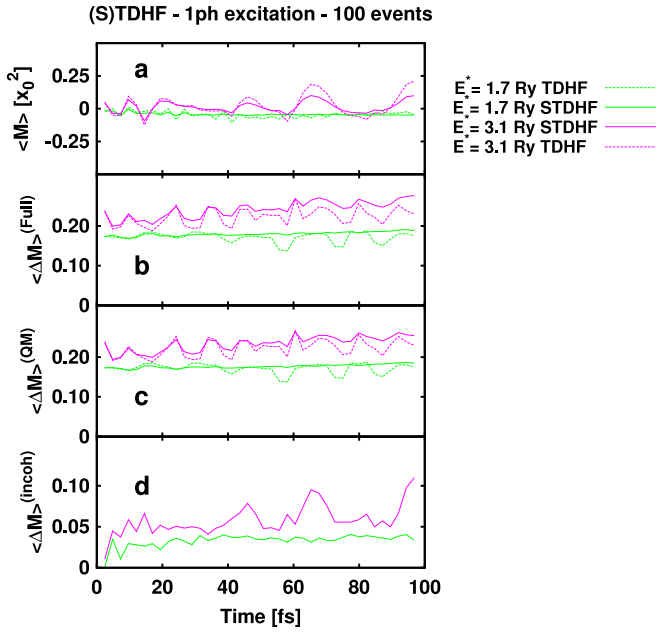

Fig. 11. Time evolution of M from Eq. (30) and its variances for two excitation energies and two cases, namely STDHF and TDHF.

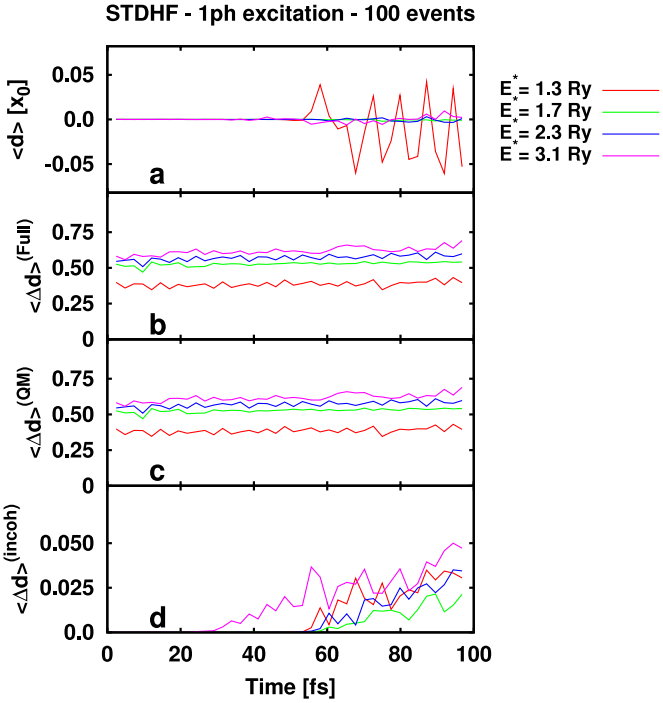

Fig. 12. Time evolution of dipole moment d from Eq. (31) and its variances for various excitation energies as indicated in the case of STDHF.

TDHF (STDHF). It incorporates dissipative effects in finite quantum systems at a microscopic level. Coherent two-body correlations are tracked for a while in time dependent perturbation theory on top of TDHF. After a certain time one reduces the coherently correlated state to a sum of mean-field states and selects one stochastically for further propagation. This is done in parallel for all states of an ensemble thus describing altogether a mixed mean-field state which eventually converges to thermal equilibrium. STDHF is applicable at sufficiently large excitation energies to allow for loss of coherence and stochastic reduction and is valid for any quantum system for which mean field provides a sound description of ground state and low energy dynamics. This is typically the case, e.g., in nuclei, molecules or clusters.

We have confined the original STDHF theory to an expansion basis of a leading mean-field state plus sufficiently large space of 2-particle-2-hole ($2ph$) states to cover the intended range of excitation energies. For first explorations, the approach has been applied to a 1D Hamiltonian modeling a small molecule. In order to analyze the emerging STDHF dynamics, we look at a couple of sensitive observables: single-particle energies and corresponding occupation numbers, one-body entropy built from the occupation numbers, one- and two-body densities, and as global observables monopole and dipole moments. For densities and moments, we also consider the variances. The entropy turns out to be the most compact and decisive criterion of thermalization. It exhibits typical relaxation pattern with a first phase of fast relaxation followed by an asymptotic one with slower relaxation. This relaxation drives correctly to thermal equilibrium as shown by snapshots of the distributions of occupation numbers which indeed converge to a Fermi function. The physical effects of thermalization were analyzed on the one- and the two-body densities. We have seen how collisional correlations smooth the quantum fluctuations of the densities. Global observables such as monopole and dipole moment, in particular their variances, do also acquire a contribution from thermalization. In this case, however, quantum fluctuations, which are already present at TDHF level, are dominating such that effects from the thermal ensemble are hard to discriminate. Occupation numbers (entropy) and detailed local distributions are clearly the more sensitive observables.

The investigations of this paper show that STDHF provides a robust tool to investigate dissipative effects in finite quantum systems. Although demanding, an extension to realistic 3D cases is conceivable because the ensemble description allows to take advantage of parallel coding. The ensemble description will also allow to handle processes with large fluctuations as, e.g., fragmentation. The present tests show that STDHF works most efficiently in an intermediate energy range. High excitation energies require increasingly large phase spaces for transitions. This sets an upper limit. The solution at such high energies is to switch to semiclassical models which are becoming valid in this regime. At the side of low excitation energies we are plagued by low transition probabilities which require larger ensembles to acquire sufficient statistics. This sets a lower limit. However, fluctuations are small at low energy: This would allow to recollect the description to one common mean field which improves the sampling. Work in this direction is in progress.

Acknowledgments

We thank Institut Universitaire de France, European ITN network CORINF and French ANR contract MUSES for support during the realization of this work.

References

[1] K. Hansen, Statistical Physics of Nanoparticles in the Gas Phase, Springer, Netherlands, Amsterdam, 2013.
[2] U. Saalmann, C. Siedschlag, J.M. Rost, J. Phys. B 39 (2006) R39.
[3] T. Fennel, K.-H. Meiwes-Broer, J. Tiggesbäumker, P.-G. Reinhard, P.M. Dinh, E. Suraud, Rev. Modern Phys. 82 (2010) 1793.
[4] M. Kjellberg, O. Johansson, F. Jonsson, A.V. Bulgakov, C. Bordas, E.E.B. Campbell, K. Hansen, Phys. Rev. A 81 (2010) 023202.
[5] G. Chen, Nanoscale Energy Transport and Conversion: A Parallel Treatment of Electrons, Molecules, Phonons, and Photons, Oxford University Press, New York, 2005.
[6] J. Dalibard, in: M. Inguscio, S. Stringari, C. Wieman (Eds.), Proceedings of the International School of Physics-Enrico Fermi, Course CXL, IOS Press, Amsterdam, 1999, p. 321.
[7] P. Wopperer, P.M. Dinh, P.-G. Reinhard, E. Suraud, Phys. Rep. 562 (205) (2015) page 1. arXiv:1407.4965.
[8] J. Pinaré, B. Baguenard, C. Bordas, M. Broyer, Eur. Phys. J. D 9 (1999) 21.
[9] T. Wada, N. Carjan, Y. Abe, Nuclear Phys. A 538 (1992) 283.

[10] Y. Abe, S. Ayik, P.-G. Reinhard, E. Suraud, Phys. Rep. 275 (1996) 49.
[11] N. Bohr, J.A. Wheeler, Phys. Rev. 56 (1939) 426.
[12] D.H.E. Gross, Microcanonical Thermodynamics, World Scientific, Singapore, 2001.
[13] G.F. Bertsch, S. Das Gupta, Phys. Rep. 160 (1988) 190.
[14] A. Bonasera, F. Gulminelli, J. Molitoris, Phys. Rep. 243 (1994) 1.
[15] L.P. Kadanoff, G. Baym, Quantum Statistical Mechanics: Green's Function Methods in Equilibrium and Nonequilibrium Problems, in: Frontiers in Physics, Benjamin, New York, 1962.
[16] D. Pines, P. Nozières, The Theory of Quantum Liquids, W A Benjamin, New York, 1966.
[17] H. Feldmeier, Nuclear Phys. A 515 (1990) 147.
[18] A. Ono, H. Horiuchi, Prog. Part. Nucl. Phys. 53 (2004) 501.
[19] K. Goeke, P.-G. Reinhard, Time-Dependent Hartree–Fock and Beyond, in: Lecture Notes in Physics, vol. 171, Springer, Heidelberg, 1982.
[20] P.-G. Reinhard, E. Suraud, Ann. Physics (NY) 216 (1992) 98.
[21] A. Domps, P.-G. Reinhard, E. Suraud, Phys. Rev. Lett. 81 (1998) 5524.
[22] T. Fennel, G.F. Bertsch, K.-H. Meiwes-Broer, Eur. Phys. J. D 29 (2004) 367.
[23] Y. Huismans, E. Cormier, C. Cauchy, P.-A. Hervieux, G. Gademann, A. Gijsbertsen, O. Ghafur, P. Johnsson, P. Logman, T. Barillot, C. Bordas, F. Lépinea, M.J.J. Vrakking, Phys. Rev. A 88 (2013) 013201.
[24] C. Cercignani, The Boltzmann Equation and its Applications, in: Applied Mathematical Sciences, vol. 67, Springer, New York, 1988.
[25] R. Balescu, Equilibrium and Non Equilibrium Statistical Mechanics, Wiley, New York, 1975.
[26] E.-A. Uehling, G.-E. Uhlenbeck, Phys. Rev. 43 (1933) 552.
[27] H. Uechi, Neutron Star Structure and Fermi-Liquid Properties of Nuclear Matter in a Relativistic Hadronic Field Theory, Indiana University, Bloomington, 1988.
[28] D. Durand, E. Suraud, B. Tamain, Nuclear Dynamics in the Nucleonic Regime, Institute of Physics, London, 2000.
[29] A. Nitzan, M.A. Ratner, Science 300 (2003) 1384.
[30] M. Bixon, R. Zwanzig, Phys. Rev. 187 (1969) 267.
[31] R. Zwanzig, J. Stat. Phys. 9 (1973) 215.
[32] S. Ayik, C. Gregoire, Phys. Lett. B 212 (1988) 269.
[33] J. Randrup, G.F. Burgio, P. Chomaz, Nuclear Phys. A 538 (1992) 393.
[34] P. Napolitani, M. Colonna, Phys. Lett. B 726 (2013) 382.
[35] A.K. Rajam, I. Raczkowska, N.T. Maitra, Phys. Rev. Lett. 105 (2010) 113002.
[36] R. Requist, O. Pankratov, Phys. Rev. A 81 (2010) 042519.
[37] A. Dutta, C. Trefzger, K. Sengupta, Phys. Rev. B 86 (2012) 085140. http://dx.doi.org/10.1103/PhysRevB.86.085140.
[38] P. Krause, T. Klamroth, P. Saalfrank, J. Chem. Phys. 127 (2007) 034107.
[39] R.M. Dreizler, E.K.U. Gross, Density Functional Theory: An Approach to the Quantum Many-Body Problem, Springer-Verlag, Berlin, 1990.
[40] M.A. Marques, C.A. Ullrich, F. Nogueira, A. Rubio, K. Burke, E.K. Gross, Time Dependent Density Functional Theory, Springer, Berlin, 2006.
[41] M.A.L. Marques, N.T. Maitra, F.M.S. Nogueira, E.K.U. Gross, A. Rubio, Fundamentals of Time-Dependent Density Functional Theory, in: Lect. Notes in Phys., vol. 837, Springer-Verlag, Berlin, 2012.
[42] D.J. Thouless, J.G. Valatin, Nuclear Phys. 31 (1962) 211.
[43] P. Ring, P. Schuck, The Nuclear Many-Body Problem, Springer-Verlag, New York, Heidelberg, Berlin, 1980.
[44] A.L. Fetter, J.D. Walecka, Quantum Theory of Many-Particle Systems, McGraw-Hill, New York, 1971.
[45] L. van Hove, Physica 21 (1955) 517.
[46] W. Greiner, Quantum Mechanics, Springer, Berlin, 2001.
[47] J.W. Serene, D. Rainer, Phys. Rep. 101 (1983) 221.
[48] C. Toepffer, P.-G. Reinhard, Ann. Physics (NY) 181 (1988) 1.
[49] K. Gütter, K. Wagner, P.-G. Reinhard, C. Toepffer, Ann. Physics (NY) 225 (1993) 339.
[50] G. Casati, G. Maspero, D. Shepelyansky, Phys. Rev. Lett. 82 (1999) 524.
[51] E. Suraud, P.-G. Reinhard, New J. Phys. 16 (2014) 063066.